Available online at www.sciencedirect.com
SCIENCE DIRECT®
Polymer 45 (2004) 3429–3440
polymer
www.elsevier.com/locate/polymer

Phase transitions and structural parameters of HIQ-40 liquid crystalline co-polyester

Georgi Georgiev[a,1], Nathan Gilfoy[a], Peggy Cebe[a,*], Malcolm Capel[b,2]

[a]*Physics and Astronomy Department, Tufts University, STC-208, 4 Colby Street, Medford, MA 02155, USA*
[b]*Biology Department, Brookhaven National Laboratory, Upton, NY, USA*

Received 10 December 2003; received in revised form 27 February 2004; accepted 2 March 2004

Abstract

We describe the impact of thermal treatment on the structure and phase transitions of the liquid crystalline aromatic co-polyester, HIQ-40, comprising 40 mol% *p*-hydroxybenzoic acid (H), 30 mol% isophthalic acid (I), and 30 mol% *p*-hydroquinone (Q). Simultaneous, real-time wide and small angle X-ray scattering (WAXS, SAXS), differential scanning calorimetry, and optical ellipsometry were used to study initially isotropic, amorphous films of HIQ-40. Films were annealed above the glass transition temperature, T_g, at temperatures, T_a, from 130 to 290 °C. Depending upon T_a, thermal treatment results in formation of regions of nematic order and/or crystalline order in a disordered matrix. As T_a increases, molecular mobility in the amorphous phase increases resulting in a reduction in T_g. Two or three endothermic events are seen in all samples by thermal analysis. The lowest temperature endotherm is associated with melting of crystals formed either at T_a or during the thermal scan. The two higher temperature endotherm features result from transformation of crystal melt-to-nematic, and formation of more mobile nematic domains from constrained liquid, respectively, and are relatively insensitive to T_a.

A strong Bragg scattering peak is seen for $T_a < 290$ °C corresponding to formation of two-phase structure comprising crystals and disordered phase. At higher temperatures, very strong scattered intensity in the SAXS pattern re-emerges, even after all WAXS crystal reflections have disappeared. Results suggest that a two-phase structure, of ordered nematic domains co-existing with less ordered regions, may be forming continuously above the crystal melting point.

Keywords: Liquid crystalline co-polyester; X-ray scattering; Nematic

1. Introduction

The structure and properties of main chain liquid crystalline polymers (LCPs) are currently of technological interest since these materials show promise for use as semi-permeable membranes, dielectric coatings, and processing aids owing to their tendency for global alignment during extrusion and injection molding [1]. Of special interest are LCPs that form crystalline order, in addition to their liquid crystalline phases [2–16], such as thermotropic co-polyesters. Depending upon chemical structure sequence, a variety of crystal types was observed by Erdemir and co-workers [3,5,10]. Blundell [2] reported that stiff chain co-polyesters produced crystals too small to be observed directly by X-ray scattering [2]. Butzbach, et al. [4] also found highly defective crystals, but suggested that the nematic melt could also serve to precondition the chains to facilitate crystallization. Increasing chain flexibility lead to highly crystalline co-polyesters that crystallized from the nematic state according to an Avrami process [8]. Thermal properties and structure of the co-polyester LCPs, such as the temperatures of transition, and ability to form crystalline phases or nematic domains, depends upon the composition ratio of co-polymer units [9,11,12,14,15].

Here we report on a study of the thermotropic liquid crystalline random co-polyester known as HIQ-40 [11,12,14]. This LCP is based on wholly aromatic, random co-polyesters of *p*-hydroxybenzoic acid (H, 40 mol%), *p*-hydroquinone (Q, 30 mol%), and isophthalic acid (I, 30 mol%) with chemical structures as shown in Scheme 1. Park, et al. [12] studied the mesogenic textures of HIQ-40

* Corresponding author. Tel.: +1-6176273365; fax: +1-6176273744.
E-mail address: peggy.cebe@tufts.edu (P. Cebe).
[1] Present address: Physics Department, Northeastern University, Boston, MA.
[2] Present address: Argonne National Laboratory, Argonne, IL.

0032-3861/$ - see front matter © 2004 Elsevier Ltd. All rights reserved.
doi:10.1016/j.polymer.2004.03.030

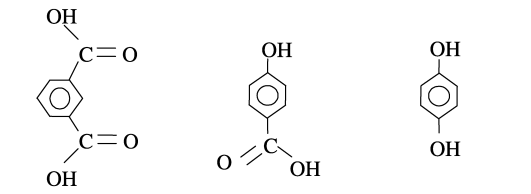

Isophthalic Acid p-Hydroxybenzoic Acid Hydroquinone

Scheme 1. Composition of HIQ-40 [2,3].

mainly because of its barrier properties. Maximum crystallinity after annealing at 300 °C is reported at 15–20%. Although the degree of true, three-dimensional crystallinity is low in these LCP materials, Makhija and Jaffe [9], through extensive studies of both controlled and partially controlled co-polyester sequences of HIQ-33 and HIQ-50, found that these LCPs exhibit crystalline order within the liquid crystalline phase when they were annealed above 250 °C. The crystal to nematic transition for HIQ-40 was reported to be between 300 and 375 °C [11].

Cantrell, et al. [14] and Menczel [11] initially studied the synthesis, thermal and qualitative optical properties of HIQ-40, and the development of nematic order above the isotropic glass transition. These researchers showed that in solution-cast film, evaporation rates were sufficiently fast that glassy, isotropic films are formed before crystals or mesogenic ordering can develop. Cantrell, et al. [14] reported that HIQ-40 exhibits two glass transitions: the first is centered around 42 °C, and is associated with the 'glass-to-rubber' transition of the disordered polymer; the second is around 110–115 °C, depending on the thermal treatment, and is associated with glass-to-rubber transition of the nematically ordered molecules. Further thermal work showed that above the melting endotherm at 307 °C HIQ-40 exhibits a fluid liquid crystalline structure [14]. The nematic to isotropic transition is above 480 °C, which is the degradation temperature of the material, and for this reason it cannot be observed. However, samples annealed at 330 °C were clearly birefringent, and these researchers conclude the existence of a nematic fluid. According to Jaffe and co-workers [9,11,12,16], the annealing of metastable isotropic films of HIQ-40 leads to a global transformation of the microstructure from isotropic to nematic structure.

In several studies [11,12,14], the phase transformation from isotropic glassy state to a state of higher molecular order (either nematic liquid crystalline order, or true three-dimensional crystalline order) could occur by heating the quenched HIQ-40 material. This thermal scheme is very similar to the process of 'cold crystallization' seen in some flexible chain semicrystalline polymers [17–20]. Provided that the glass transition is high enough in temperature, the semicrystalline polymer can be quenched from the melt directly into a glassy isotropic state at room temperature. Heating above the glass transition causes the crystalline phase transformation to occur as chains gain the necessary mobility. Here we conduct a systematic exploration of the effects of 'cold annealing' applied to HIQ-40 quenched isotropic glassy films. Films are annealed at temperatures ranging from just above the upper T_g to within the crystalline melting range, in order to study the formation of ordered structures including nematic domains and three-dimensional crystals, and their subsequent phase transformations upon re-heating.

The sequence of formation of ordered structures in the crystallizable LCPs should depend upon whether the sample is cooled from isotropic liquid, or heated from isotropic glass. In the first case, upon cooling to room temperature, the transition sequence for forming (non-equilibrium) ordered structures is expected to be: isotropic liquid → nematic liquid crystal → crystal. Here the arrow may be read as 'becomes' or 'transforms into'. Due to mobility restrictions and incomplete conversion between the phases, below the glass transition the LCP sample may contain crystals, nematic regions, and isotropic glassy regions. In the second case, upon heating from room temperature, the transition sequence for forming (non-equilibrium) ordered structures from quenched glassy material is: isotropic glass → isotropic liquid → nematic liquid crystal → crystal. Then, we anticipate that further heating will melt the crystals and provide mobility so that the ordered structures become disordered in the following sequence as temperature increases: crystal melt → nematic liquid crystal → isotropic liquid. Using several investigative methods, we study the order/disorder sequence of HIQ-40 LCP.

Because the hierarchy of structures for LCPs spans many length scales, a variety of approaches is needed for complete description of the morphology. Optical microscopy or small angle light scattering are used to study formation of large domains, on the micron size scale. Small- and wide-angle X-ray scattering (SAXS and WAXS) can be utilized to examine the periodical arrangement of crystals, including formation of crystalline stacks. An advantage of the X-ray scattering techniques is that they can be performed at elevated temperature using high intensity synchrotron sources, to observe the formation and disappearance of ordered structures in real-time. To our knowledge, no small angle X-ray scattering work has yet been undertaken on HIQ-40. Here, we employ simultaneous WAXS and SAXS, temperature-modulated differential scanning calorimetry (TMDSC), and two-dimensional optical ellipsometric studies (a variant of polarized light microscopy), to assess the effect of annealing temperature on the thermal and structural properties of HIQ-40. Annealing of HIQ-40 results in formation of a complex structure that includes crystals coexisting with both ordered nematic domains and disordered, isotropic liquid.

2. Experimental section

Initial preparation of HIQ-40 films from solution, and

characterization of the chain structure, has been reported previously [14]. The authors verify [14] the random nature of the co-monomer units in HIQ-40 based upon NMR studies. Glassy isotropic amorphous bulk films of HIQ-40, around 10 μm thick, were kindly provided by Professor Benny Freeman. Bulk films were isothermally annealed at temperatures, T_a, in the range 130–290 °C for 1 h in a Mettler FP80 microscope hot stage, cooled at 5 °C/min to room temperature, and then analyzed using thermal analysis or X-ray scattering. We performed calorimetric studies of HIQ-40 using a TA Instruments 2920 TMDSC. Samples were scanned at 5 °C/min, with modulation amplitude of 0.796 °C and modulation period of 60 s. For the TMDSC studies, the film was cut and stacked to provide sufficient mass, around 2 mg, for signal detection. Melting peak temperatures and heats of fusion were calibrated using indium standard. Nitrogen purge gas was used at a flow rate of 30 ml/min.

Real-time SAXS and WAXS were used to follow development of the scattering invariant, long periodicity, crystal thickness and crystalline lattice peaks and scattering from the nematic phase. SAXS and WAXS were performed simultaneously at the Brookhaven National Synchrotron Light Source, beam lines X12B and X27C. The latter system was equipped with two one-dimensional gas-filled wire detectors. The X-ray wavelength, λ, was 0.1366 nm, beam diameter was 300 μm (treated as a pinhole source), and the sample to detector distance was about 180.0 cm. Calibration of the scattering vector, s ($s = 2 \sin\theta/\lambda$ where θ is the half scattering angle), was done using silver behenate for SAXS, and sodelite for WAXS. Intensity data were taken continuously during heating at 5 °C/min from 100 to 375 °C, with samples held inside the Mettler FP80 hot stage. Each scan was collected for 60 s.

The SAXS raw intensity was corrected for background subtraction, sample absorption, changes in incident beam intensity, and thermal density fluctuation from Is^4 vs. s^4 plots [21]. Structural parameters were determined on the basis of a two-phase model, from the one dimensional electron density correlation function, $K(z)$, obtained by discrete Fourier transformation of the Lorentz corrected intensity, Is^2, using [22,23]:

$$K(z) = \sum_{j=1}^{N} 4\pi s^2 I(s) \omega_N^{(j-1)(z-1)} \quad (1)$$

where $\omega_N = \exp(-2\pi i/N)$ and N is the actual number of data points. z is the direction normal to the periodic stacks. The Bragg long period, L_B, scattering invariant, Q, and crystal thickness, L_c, were determined from $K(z)$ according to the method of Strobl and Schneider [24].

The total integrated area, also called the scattering invariant, Q, is given by Ref. [21]:

$$Q = \int_0^\infty 4\pi s^2 I(s) \mathrm{d}s \quad (2)$$

where I is the intensity after all corrections. Assuming a two-phase scattering model, this integral is also related to the volume fractions of the two phases, ϕ_1 and ϕ_2 (where $\phi_2 = 1 - \phi_1$) and the difference in electron density between the phases, $\rho_1 - \rho_2$ (in units of electrons per volume), through the general expression:

$$Q = \phi_1(1 - \phi_1)(\rho_1 - r_2)^2 \quad (3)$$

Finally, two-dimensional optical ellipsometry was performed using the experimental set-up of polarized light microscopy described previously [25,26] following an approach developed by Oldenbourg and Mei [27]. The technique uses Stokes analysis of the polarization of transmitted light [28] to measure the optical retardation, δ, of the sample in terms of wavelength, λ, thickness, d, and birefringence, Δn ($= |n_e - n_o|$) from $\delta = (2\pi/\lambda)d\Delta n$. Birefringence develops in the films as a result of crystallization or formation of liquid crystalline ordering. The optical intensity was measured in real time as the sample was heated. For preparation of samples for ellipsometry, one layer of film was floated on a water droplet onto a glass slide and dried flat.

3. Results and discussion

3.1. Thermal analysis

Thermal analysis results are shown in Figs. 1 and 2. In Fig. 1(a) and (b), TMDSC total heat flow curves vs. temperature are shown for HIQ-40 as-received, or annealed for 1 h at the temperatures, T_a, listed adjacent to the curves. In the non-pretreated film ($T_a = 25$ °C) the first feature detected is the crystallization exotherm, while in the pretreated films (Fig. 1(a), $T_a = 130$–140 °C), the first

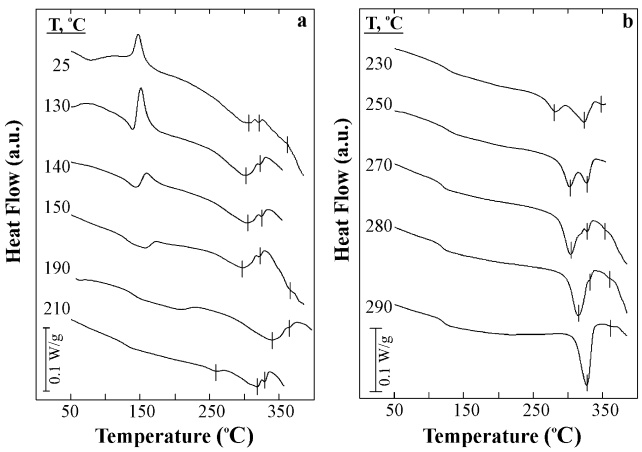

Fig. 1. TMDSC total heat flow vs. temperature for HIQ-40 non-pretreated sample ($T = 25$ °C) or samples annealed for 1 h at the indicated temperatures, T_a. (a) Lower T_a. (b) Higher T_a. The vertical lines mark the locations of endothermal events above the glass transition temperature. Endotherms are represented by downward deflection of the heat flow from the baseline.

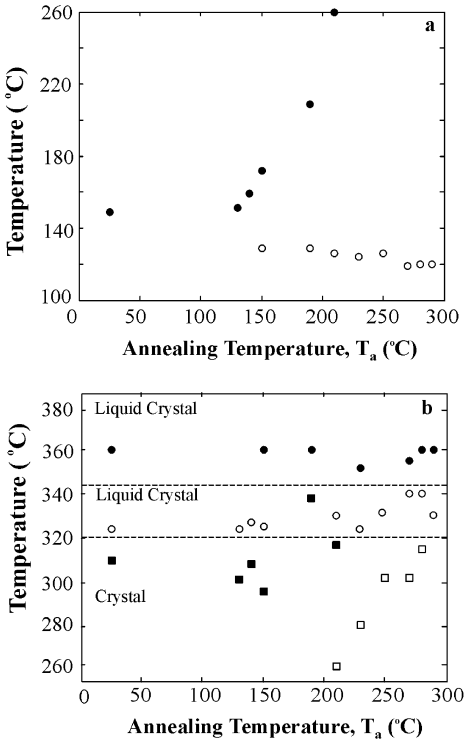

Fig. 2. Thermal transition temperatures vs. annealing temperature for HIQ-40 from the TMDSC total heat flow curves. (a) Glass transition temperature, T_g (open circles), crystallization temperature, T_c (filled circles). (b) Peak locations of endothermic events: Nematic liquid crystal domains (filled circles); crystal melt-to-nematic liquid crystal (open circles); crystal melting (squares). Melting of pre-existing crystals and crystals formed during the DSC scan (filled squares); melting of crystals formed during the annealing treatment (open squares).

feature measured is the start of the glass transition temperature, which occurs initially around 120 °C. For the samples pre-treated at those relatively low T_a, scanning in the calorimeter results in immediate exothermic heat flow when T_g is exceeded. The glass transition is barely seen as an increase in the heat capacity and no high temperature heat capacity plateau can be seen due to the overlap with the crystallization exotherm.

A clear step transition at T_g is first seen in the scans of samples isothermally annealed for 1 h at and above 150 °C, where there is no immediate re-crystallization happening to mask the T_g. Dependence of thermal transition temperature on T_a is shown in Fig. 2(a) and (b) with values listed in Table 1. As shown in Fig. 2(a), T_g (open circles), decreases slightly with increasing annealing temperature while the crystallization temperature, T_c (filled circles), increases sharply. The crystals introduced at the annealing temperature apparently restrict the amorphous phase in a manner dependent upon T_a. The constraints exerted by the crystals are most severe at low T_a, where the amorphous phase has the least mobility, resulting in highest values of T_g. As T_a increases, molecular mobility in the amorphous phase improves, and the constraints of the crystals upon the amorphous phase are less severe, resulting in a reduction in T_g.

Table 1
Characteristic temperatures of HIQ-40 from TMDSC total heat flow as a function of annealing temperature T_a : glass transition, T_g; crystallization exotherm peak, T_c; endothermal peaks, T_m, T_{lc1}, T_{lc2}

T_a (°C)	T_g (°C)[a]	T_c (°C)[a]	T_m (°C)[a]	T_{lc1} (°C)[a]	T_{lc2} (°C)[b]
25 (Non-pretreated)	n	149	310	323	360
130	n	151	303	323	–
140	n	159	308	326	–
150	129	172	296	323	360
190	129	209	338	n	360
210	126	260	257, 317	330	–
230	124	n	281	323	350
250	126	n	305	330	–
270	119	n	305	340	355
280	120	n	315	340	360
290	120	n	n	330	360

T_m : crystal melting; T_{lc1} : crystal melt-to-nematic; T_{lc2} : nematic domains.
[a] n indicates that no feature of this type was observed in the scan.
[b] Dash indicates that TMDSC data collection was carried out only to 350 °C.

This result is similar to that observed in some semicrystalline thermoplastic polymers of low crystallinity, such as PEEK [18,29] and PPS [30,31]. One difference is that the reduction in T_g as T_a increases, is greater in HIQ-40 than in either PEEK or PPS for similar range of cold crystallization temperatures. In HIQ-40, T_g decreases by about ten degrees over the entire range of annealing temperatures. For similar range of cold crystallization temperatures, PEEK glass transition decreased less than five degrees [29]. The glass transition of PPS decreased also by less than five degrees over a smaller range of cold crystallization temperatures [30,31]. Thus, the effect of low temperature annealing on HIQ-40 is to increase T_g by about ten degrees compared to the value achieved at the highest annealing temperatures.

Recrystallization exotherms are observed in the heating scans of samples pretreated up to temperature of 210 °C (solid circles in Figure 1(a)). A strong exothermic peak occurs for samples treated up to 140 °C, while in the samples treated in the range 150–210 °C only a broad exothermic deflection of the baseline signifies crystallization. As T_a increases, the crystallization exotherm decreases in area, and shifts towards higher temperatures. For the samples pretreated at temperatures above 210 °C, no re-crystallization is seen because of the growth of a low temperature endotherm, T_m, (squares in Fig. 2(b)) which hides any exotherm. For annealing temperatures in the range 230–290 °C, the low temperature endotherm, T_m, grows in area and its peak temperature increases as T_a increases.

The thermal behavior shown in Fig. 1 is quite complex, including melting of crystals formed during the scan, melting of crystals formed at the annealing temperature, reorganization of crystals during the scan, and crystal to liquid crystal endothermic transitions. The effect of cooling rate after annealing was not explored in the present work,

but it is likely that rate could be a significant factor affecting the structure observed at room temperature. This would be especially important at the highest annealing temperatures, where molecular mobility is greatest.

The thermal transitions are assigned based on: (1) relative position of the endotherm, (2) relationship to annealing temperature, and, (3) correspondence with X-ray scattering results (to be presented later). In Fig. 2(b), crystalline endothermic transitions are shown with squares, and liquid crystalline transitions are shown with circles. Two horizontal lines are drawn to separate and categorize the endothermic events. One line is drawn at about 343 °C; above this temperature only the nematic liquid crystal phase is observed. A lower line is drawn at about 320 °C; below this temperature, only crystalline melting transitions are observed. In between, predominantly the crystal melt-to-nematic transition occurs, but in the case of the sample annealed at 190 °C, the crystal melting endotherm overlaps the liquid crystalline transition point. No nematic to isotropic transition was seen in any of the samples we studied.

All samples display one to three endothermic events whose locations depend on the treatment temperature, as shown in Fig. 2(b). The thermal scans of the samples non-pretreated or treated at temperatures at and below 190 °C (refer to Fig. 1(a)) show a first broad endotherm (crystal melting), followed by a second higher temperature small endotherm (transition from crystal to nematic state). The location of the first endotherm is not strongly dependent upon the annealing temperature for $T_a \leq 190$ °C.

For the samples pretreated at higher annealing temperatures, $T_a > 190$ °C, the TMDSC scans (Fig. 1(a) and (b)) show a crystal melting endotherm forming at a temperature lower than the original one seen in samples treated at lower annealing temperatures. This endotherm changes both in position and in magnitude, shifting towards higher temperatures and larger area, with the increase of T_a. We attribute this endotherm to melting of crystals formed during the long annealing time at elevated temperatures. For treatments above 230 °C, the crystal to nematic transition appears as a clear, small higher temperature endotherm, at T_{lc1}, above the melting endotherm. In the sample annealed at 290 °C, the crystal melt-to-nematic transition at T_{lc1} is the major endothermic event.

Most of the samples were heated to a temperature above 350 °C. In all samples so treated, an additional third endothermic event can be seen (solid circles in Fig. 2(b)). The appearance of this feature is either as a very weak endothermic peak or as a slope change in the heat flow trace. This feature is nearly independent of annealing temperature. It appears always at temperatures above the melting temperature of the crystal population and thus is associated with a liquid crystal transition, T_{lc2}, occurring near 360 °C in most samples.

Since the wide temperature scaling on Fig. 2 prevents accurate determination of the peak transition temperatures, these are listed for convenience in the last three columns of Table 1. Although all samples do exhibit endothermic events associated with crystal melting, it must be appreciated that the levels of crystallinity that develop are always quite small as will be shown in the next section on wide angle X-ray scattering.

3.2. Wide angle X-ray scattering

Real-time wide-angle X-ray scattering intensities vs. scattering angle are shown in Fig. 3 for a representative sample, HIQ-40 annealed for 1 h at 230 °C. The scans were taken from 100 °C, just below the glass transition temperature, to 375 °C, the upper limit temperature of our hot stage, at heating rate of 5 °C/min. Two crystalline WAXS peaks appear at $2\theta = 14.37°$ and 23.54° for $\lambda = 0.1336$ nm with d-spacings according to Bragg's law of 0.53 and 0.33 nm, respectively. During heating, the crystalline reflections begin to disappear by 260 °C, just at the start of the lower melting endotherm, and they are completely melted by 280 °C where the endotherm has its peak position. A sharpened halo peak, characteristic of the nematic liquid crystalline phase, occurs after the crystals have melted. Upon further heating to 350 °C the liquid crystalline reflection broadens to a halo typical of more disordered material.

Fig. 4 shows the collected WAXS scattering patterns of HIQ-40 during heating, at selected elevated temperatures of 100 °C (Fig. 4(a)), 200 °C (Fig. 4(b)), 300 °C (Fig. 4(c)), and 370 °C (Fig. 4(d)). The same four sample treatments are compared in all portions of the figure. Curve 1 is the sample non-pretreated; curves 2, 3, and 4 are samples annealed for 1 h at 150, 230, or 290 °C, respectively. With an increase of temperature, the crystalline peaks decrease and once the melting temperature is exceeded, they disappear completely.

Arrows mark the crystalline reflections in parts (a) and (b) of Fig. 4. These are the same peaks as reported in Ref. [14], corresponding to the crystal form C, with d-spacings

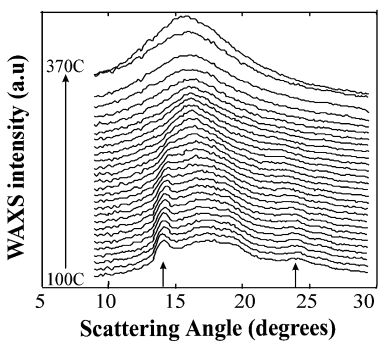

Fig. 3. WAXS intensity vs. scattering angle (at $\lambda = 1.366$ Å) for HIQ-40 annealed at 230 °C, and then heated from 100 to 370 °C at 5 °C/min. Each scan was of 1 min. duration and the scans represent 10 °C intervals. The temperature of each scan represents the initial temperature at which intensity was collected.

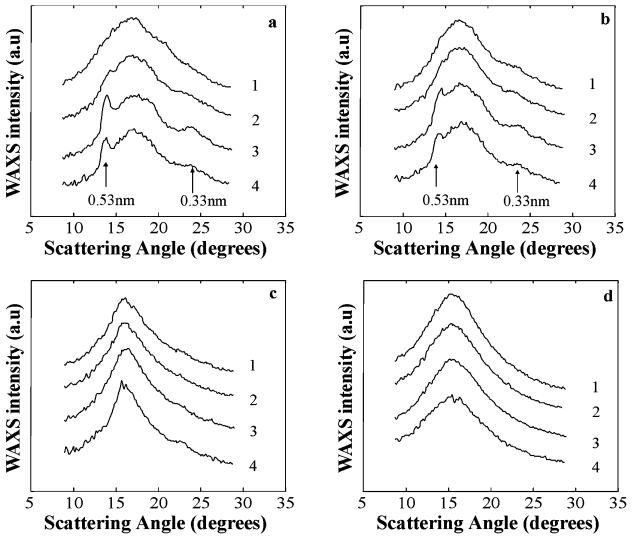

Fig. 4. Real-time WAXS intensity vs. scattering angle (at $\lambda = 0.1366$ nm) for HIQ-40 taken at selected elevated temperatures of: (a) 100 °C; (b) 200 °C; (c) 300 °C; (d) 370 °C. Non-pretreated sample (curve 1). Sample annealed for 1 h at 150 °C (curve 2), 230 °C (curve 3), or 290 °C (curve 4).

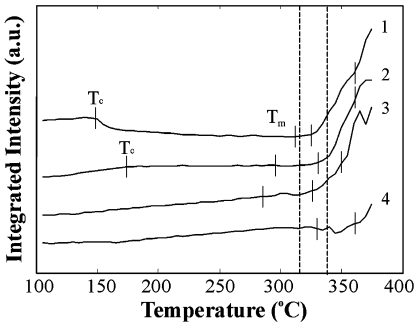

Fig. 5. Integrated WAXS intensity vs. temperature of HIQ-40. Non-pretreated sample (curve 1); sample annealed at 150 °C (curve 2), 230 °C (curve 3), or 290 °C (curve 4). For comparison, short vertical lines mark the temperatures of TMDSC thermal transitions such as crystallization exotherm, T_c, and crystal melting, T_m, and liquid crystalline endothermal events. The vertical dashed lines correspond to the same boundaries marked in Fig. 2(b). Curves are displaced vertically for clarity.

reported at 0.52 and 0.33 nm. According to these researchers the crystalline order can be attributed to the regular Q-I sequences. Another characteristic feature is that the peaks in the WAXS region are broad and weakly expressed. Clear crystalline peaks exist only for samples isothermally annealed for 1 h at 230 and 290 °C. The non-pretreated sample and the one annealed at 150 °C show no strong crystal peaks, however the latter sample shows a weak peak around $2\theta = 14°$. Absence of strong, sharp WAXS reflections implies that the crystals are small, imperfect, and not numerous.

Above the temperature of the first endotherm (in Table 1 the column marked as T_m), the crystalline structures seen in the WAXS scans disappear. Then the formerly broad WAXS peak becomes noticeably sharper (Fig. 4(c)), because of the presence of liquid crystalline structures [4,11,14]. As temperature increases further, to temperatures above the upper dashed line in Fig. 2(b), the peak broadens again (Fig. 4(d)).

Using real-time WAXS, we can follow qualitatively the disappearance of the crystalline peaks during heating through the same temperature range used in the thermal studies. Integrated WAXS intensity (total curve area, from $2\theta = 9–35°$) during heating is shown in Fig. 5 for HIQ-40 non-pretreated sample (curve 1) and samples annealed at 150 °C (curve 2), 230 °C (curve 3) and 290 °C (curve 4). The short vertical lines call attention to important thermal transition temperatures observed in TMDSC analysis of these samples. The integrated WAXS scans show a change in the slope at the crystallization temperature for two samples: non-pretreated (curve 1) and the sample annealed at 150 °C (curve 2). The samples annealed at 230 °C (curve 3) or 290 °C (curve 4) show no change in the slope in the temperature range before melting. The biggest change in slope for these samples is seen only after the endotherm associated with the crystal melt-to-nematic transition (i.e. above the dashed line at higher temperature).

3.3. Small angle X-ray scattering and optical studies

Real-time SAXS intensity was monitored as the samples were heated from 100 to 370 °C, to determine the creation and disappearance of long range ordered structure. Fig. 6 shows contour plots of the Lorentz-corrected SAXS intensity vs. scattering vector, $s(s = 2 \sin\theta/\lambda = q/2\pi)$, vs. temperature during heating at 5 °C/min. A cyclic color scale was used to indicate the relative intensity, for presentation purposes, so that both the stronger and the weaker peaks could be seen together on the same figure. The total intensity range was divided into either two cycles (Fig. 6(a), (b) and (d)) or three cycles (Fig. 6(c)), with blue referring to the least intense and red the most intense within the cycle. The intensity shown in Fig. 6 should be viewed as a qualitative one, since the division between cycles was arbitrarily chosen. In all parts of the figure, intensity increases from upper right side to the lower left side, and temperature increases in the direction of the vertical arrow.

The Bragg peak from periodic structures is well expressed in the SAXS scans for most of the samples (Fig. 6(a)–(c)), but not the one crystallized isothermally at 290 °C (Fig. 6(d)). For the non-pretreated sample (Fig. 6(a)) there is no SAXS peak visible before 160 °C because the sample is initially non-crystalline. After the crystallization exotherm, the Bragg scattering is seen to develop by 200 °C. The peak at $s = 0.06$ nm^{-1} corresponds to a Bragg period of 16.0 nm. As temperature increases, the peak position continuously shifts to lower s-value, while strengthening in intensity. SAXS shows significant intensity still remaining at 320 °C above the endotherm peak at T_m (from Table 1, $T_m = 310$ °C), and above the temperature where the WAXS peaks have disappeared. The intensity at low s-value appears to drop at about 335 °C, and the Bragg peak is no

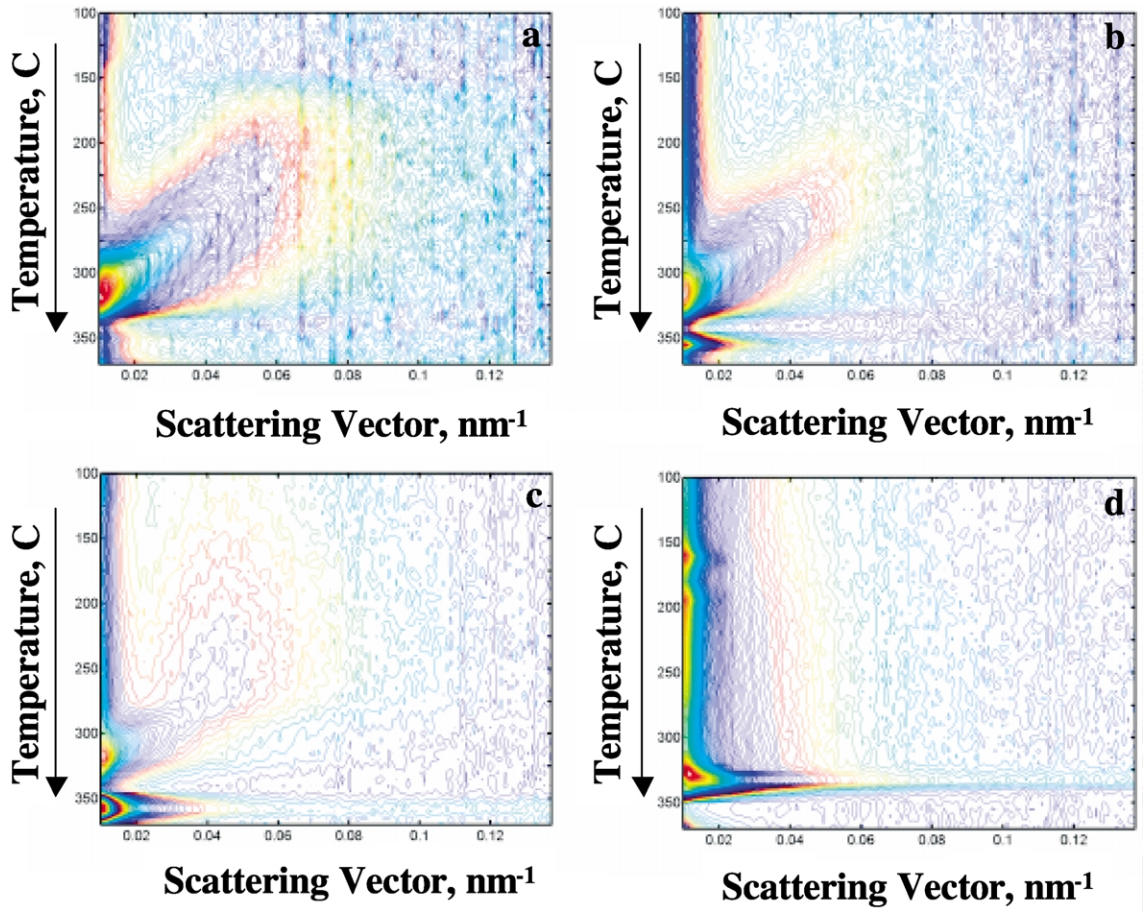

Fig. 6. Contour plots of Lorentz-corrected SAXS intensity vs. temperature vs. scattering vector, s ($s = 2 \sin \theta/\lambda$, $\lambda = 0.1366$ nm), for HIQ-40 during heating at 5 °C/min. Temperature increases from top to bottom in the contour plots as indicated by the arrow. (a) Non-pretreated sample; samples annealed for 1 h at: (b) 150 °C; (c) 230 °C; (d) 290 °C. The relative scattered intensity is represented by a color scheme that varies from blue (least intense) to red (most intense). Intensity increases cyclically from upper right side to the lower left.

longer seen above that temperature. With continued heating, additional scattered intensity at low s-value develops once again, with a broad distribution above 345 °C.

Fig. 6(b) shows the contour plot of HIQ-40 annealed at 150 °C. There is already a weak Bragg peak seen in this semicrystalline sample at 100 °C, and once again the Bragg peak position shifts continuously to lower s-value as temperature increases. Up to 337 °C the SAXS scan is qualitatively similar to that of the non-pretreated sample, but the Bragg peak is narrower in this sample than in the one that was not pretreated. Above 337 °C, intense SAXS scattering at low s-value occurs in the form of a narrow 'streak' whose intensity peaks at 350 °C, above the location of the endothermic transition from crystal to nematic phase. The intensity in the streak drops off at temperature increases to 370 °C.

The sample treated at 230 °C is shown in Fig. 6(c). The Bragg scattering peak (at about $s = 0.05$ nm^{-1}) maintains a constant s-value during much of the heating, and major melting does not begin until about 281 °C (the location of the crystal melting peak in Table 1). Above the melting point, the Bragg peak shifts to a much higher s-value, and the intensity strengthens and then peaks around 312 °C as the nematic phase forms. Intensity drops at 337 °C, then returns again in the form of the streak at low s-value above 350 °C.

The sample annealed at 290 °C (Fig. 6(d)) has no typical Bragg scattering peak from periodic crystal stacks, despite the fact that WAXS (see Fig. 4) shows crystalline reflections for this sample. During heating, intensity near the low-s regions appears to strengthen around 160 and 190 °C, with a drop in intensity at 180 °C, but this is not correlated with any features seen in the TMDSC scan. On the other hand, polarizing optical analysis (to be presented later in the next section) shows slight decrease of transmitted intensity near 180 °C indicating a change in polarization of the sample. This is most likely due to some crystal melting. As temperature increases further, a very intense streak-like scattering feature strengthens at low s-value, around $s \sim 0.015$ nm^{-1}, corresponding to spacing of 65 nm. The streak is spread out across a wide range of s-values. The low-s peak is due to nematic liquid crystalline ordered structures (domains) that exist in regions of average size scale 65 nm.

To investigate the small angle scattering quantitatively,

correlation function analysis was undertaken to obtain the Bragg period, phase thickness, and scattering invariant. These results are shown in Figs. 7–9, respectively. The correlation function was used to determine the Bragg period, L_B, for the higher-s peak (arising from crystal stacks) using Eq. (1), and these results are shown in Fig. 7. The sample that was not annealed before the thermal scan shows its Bragg peak (triangles) for the first time at 160 °C, just above the crystallization temperature of 150 °C observed for this sample. During heating, the Bragg long period increases, as melting occurs. For the non-pretreated sample (triangles), the long period begins to increase at a slightly lower temperature than all of the other treatments. The crystals formed in this sample during heating are less perfect crystals, have smaller thickness, and are more subject to reorganization during heating. Consequently crystals in the non-pretreated sample melt at a slightly higher temperature (310 °C) than the crystals of the annealed samples (which melt below 300 °C).

The sample annealed at 150 °C (Fig. 7, stars) already has some crystalline structure when examined at 100 °C, and shows a Bragg scattering peak that starts to increase due to crystal melting, at a slightly higher temperature than the non-pretreated one. Among the three treatments (non-pretreated, annealed at 150 °C, or annealed at 230 °C) the sample that has been annealed at 230 °C (open circles) shows the highest initial Bragg long period, which is stable until higher temperature.

All three samples (non-pretreated, or annealed at 150 or 230 °C) show a sharp increase in SAXS periodicity as the crystals are melting. During the melting endotherm, the SAXS spacing increases from the initial low value of Bragg long period (20 nm or less) to a much larger value. As some thinner, least perfect crystals melt, those remaining are more widely scattered and have larger Bragg spacing.

Phase thickness, determined from the correlation function [24], is shown in Fig. 8(a) and (b). For samples showing a Bragg scattering peak (non-pretreated sample, or annealed at 150 or 230 °C), the phase thickness will be the smaller of the two lengths referring either to the crystal thickness, L_1, or to the disordered phase thickness, L_2 (where

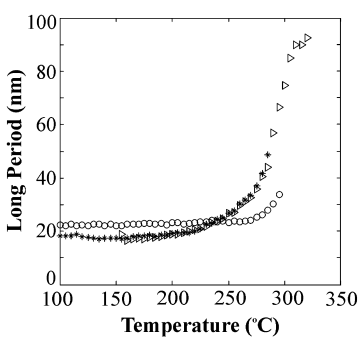

Fig. 7. SAXS long period vs. temperature for HIQ-40 non-pretreated sample (triangles); sample annealed at 150 °C (stars), or 230 °C (open circles).

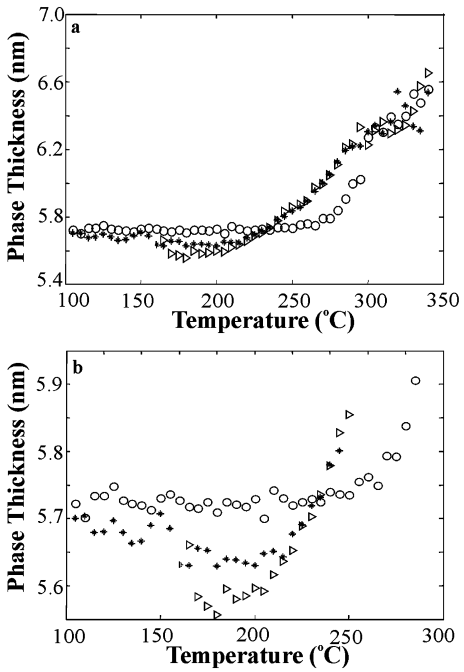

Fig. 8. SAXS characteristic thickness of phase 1 (assigned to the smaller thickness) vs. temperature for HIQ-40 non-pretreated sample (triangles); sample annealed at 150 °C (stars), or 230 °C (open circles). (a) Compressed scale. (b) Expanded scale.

$L_1 + L_2 = L_B$). By Babinet's principle of reciprocity, we have no way to distinguish between these two dimensions [21,22]. Because of the low degree of crystallinity in HIQ-40, we arbitrarily assign the smaller of the two lengths to the crystal phase, L_1. The linear stack crystallinity, χ_{cl}, may be estimated from $\chi_{cl} = L_1/L_B$ [24]. This results in a value of ~0.30 for χ_{cl} at 100 °C.

As a function of temperature, the phase thickness, L_1, shows similar behavior to the long period. The non-pretreated sample (Fig. 8, triangles) shows the smallest thickness with crystals appearing for the first time after the crystallization temperature of 150 °C. From TMDSC results, the crystals in this sample disappear due to melting of the least perfect structures, at 310 °C. The samples

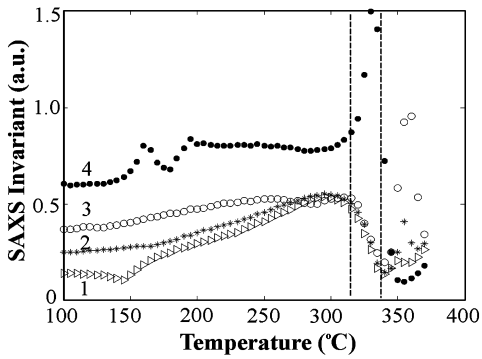

Fig. 9. SAXS Scattering invariant (total integrated intensity) vs. temperature for HIQ-40 non-pretreated sample (curve 1, triangles); sample annealed at 150 °C (curve 2, stars), 230 °C (curve 3, open circles), or 290 °C (curve 4, filled circles).

annealed at 150 °C (Fig. 8 stars) or 230 °C (Fig. 8 open circles) show larger crystal thicknesses, compared to the non-pretreated sample, which exist at 100 °C at the beginning of the scan. These crystals melt at a temperature higher than that of the crystals of the non-pretreated sample. Above 300 °C, the crystal thickness of the samples (non-pretreated, or annealed at 150 or 230 °C) increases to large values. The changes in thickness are too large (greater than 10%) to be accounted for on the basis of thermal expansion.

Fig. 9 shows the total integrated scattering intensity, or scattering invariant, Q, determined from Eq. (2). At the start of the heating, the invariant increases in the same order as the annealing temperature, with the 290 °C (solid circles) sample having the largest invariant and the non-pretreated sample (triangles) the smallest invariant. For the non-pretreated sample, and the one annealed at 150 °C (stars), Q shows a change in slope at places where the TMDSC presents a crystallization exotherm. Q increases as temperature increases due to effects both of thermal expansion, which improves the scattering contrast, and of crystallization, which increases the number of scattering entities. For the samples exhibiting a clear Bragg peak (non-pretreated, triangles; annealed at 150 °C, stars; or annealed at 230 °C, open circles) Q decreases at temperatures corresponding to the melting endotherms. After melting, in these three samples Q has a minimum, and then it increase once again, due to the existence of large-scale structures (as seen at low-s value in the contour plots in Fig. 6).

During heating, the sample annealed at 290 °C (filled circles) exhibits a change in Q from about 150–190 °C. This corresponds to the region during which small imperfect crystals melt and reorganize. This transition contributes insignificantly to the thermal scans (almost no change in baseline is seen in Fig. 1(b)), indicating that there is no net latent heat associated with the event. Above this point, the sample shows almost no change of scattered intensity, up to about 300 °C. Then Q begins to increase strongly, corresponding to the emergence of the low-s peak. The streak-like peak drops in intensity from 325 to 351 °C (see Fig. 6(d)) and then Q also drops sharply.

Small angle scattering is not associated with the nematic liquid crystalline state [32]. Nematics exhibit orientational ordering, but not positional ordering of the center of mass of the molecules, such as that seen in the crystalline phase or in smectic liquid crystals. Existence of strong scattering in the small angle range implies the formation of two-phase structures characterized by regions that differ in their electron densities [21]. The continuous increase of the Bragg spacing (for samples non-pretreated, or annealed at 150 or 230 °C), accompanied by decreasing peak intensity, is typical for melting behavior of polymer crystals. Bragg spacing shifts to higher d-spacing (smaller s-value) as crystals melt, and the peak intensity decreases as the total number of scattering entities is reduced (for examples, see Refs. [29,33,34]). The decrease in the invariant occurs mainly between the dashed lines (Fig. 9, curves 1, 2, and 3) as crystals melt and the transition to the nematic state occurs. In these samples, the scattered intensity at low-s increases once again above the upper temperature dashed line, and strongly peaks for the samples annealed at 150 and 230 °C. This signifies the re-emergence of two-phase structure, resulting from regions that differ in electron density, forming in the nematic. According to Cantrell, et al. [14], different levels of local axial order and global axial order characterize the nematic state. The axial order refers to the orientation of the director of the liquid crystal molecule [1]. While their description [14] was applied to the conversion of HIQ-40 glassy isotropic material into a nematically ordered one, the concept of different nematic regions can be applied in the present case.

We suggest that crystals originally formed in regions that were the most mobile at the formation temperature. Disordered regions separate these crystals from each other (leading to observation of the Bragg period). Upon heating, the crystals melt by disruption of the van der Waals forces between lateral chain segments. These just-melted crystals are likely to evolve most quickly into the first locally ordered nematic phase. This phase may be separated into domains by the disordered regions that separated the crystals originally. Only when the temperature increases above about 350–360 °C, are these disordered regions finally incorporated into the ordered nematic state. Then the two-phase structure disappears and a more uniform nematic results.

Optical studies were undertaken first, to measure quantitatively the integrated optical intensity for comparison to SAXS invariant, and second, to determine whether large size scale domains could be seen (on the order of microns). In Fig. 10, the optical transmitted intensity, under condition of total extinction of left circularly polarized light, is plotted as a function of temperature during heating. Prior to thermal annealing, all films were optically isotropic and appeared black under our polarization conditions. After thermal treatment, birefringence develops in the annealed samples. Optical examination showed that there is strong

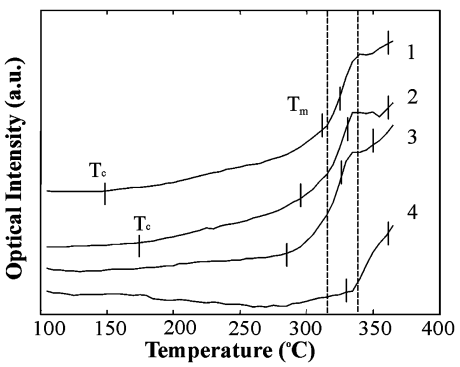

Fig. 10. Integrated transmitted polarized light intensity vs. temperature for HIQ-40 non-pretreated sample (curve 1); sample annealed at 150 °C (curve 2), 230 °C (curve 3), 290 °C (curve 4). For comparison, vertical lines at the crystallization exotherm, T_c, and endothermal events show the locations of thermal transitions. Curves are displaced vertically for clarity.

birefringence but absence of any structures on the optical scale (microns) at 100 °C for the samples treated at 150 °C (curve 2) or 230 °C (curve 3). No domains or large-scale aggregates were observed optically, indicating that the crystals formed are quite small (on the sub-micron scale) and imperfect, a fact confirmed by the absence of strong or sharp WAXS peaks. The optical intensity shows change in slope at the crystallization temperatures identified according to TMDSC studies, for the non-pretreated sample (curve 1) and the sample annealed at 150 °C (curve 2). For these two samples, as the temperature increases to the melting point, intensity continues to increase, steeply between the dashed lines, and less steeply above the upper temperature dashed line. The increase in intensity arises because of the formation of axially ordered, nematic liquid crystalline regions.

The sample annealed at 230 °C (curve 3) shows almost no change of slope in the temperature range where the long period was seen to be stable (i.e. where there was no change in L_B). At the melting point, the intensity starts to increase, continues through the crystal-to-nematic transition, and above the upper temperature dashed line, the slope changes more gradually.

The sample annealed at 290 °C behaves differently, showing a downward trend in intensity beginning at about 180 °C continuing up to about 290 °C. The optical intensity starts to increase again once the annealing treatment temperature is exceeded, and a steep change of slope occurs above the upper temperature dashed line.

The three samples, non-pretreated, and pretreated isothermally at 150 and 230 °C, do not show large-scale structures, when observed using optical ellipsometry. No domains were seen at any temperature, and no threaded nematic structure was observed [1,32]. This suggests that in nematic state, HIQ-40 forms only small-scale (less than a micron) ordered domains in those samples.

The sample that has been annealed at 290 °C (Fig. 10, curve 4) has already formed birefringent liquid crystalline phase, and it persists during the heating scan, so the retardance is initially at higher value, and does not increase during the scan as was the case for the lower temperature samples. The main increase of the optical retardance occurs after 310 °C when the sample forms a more widespread nematic liquid.

3.4. Model of structure formation

As mentioned earlier, the sequence of formation of ordered structures in the crystallizable LCP HIQ-40 depends upon whether the sample is cooled from the isotropic liquid, or heated from the isotropic glass. The two glass transitions observed were assigned as: (1) lower T_g, representing the transition from glass to rubber, of the disordered optically isotropic polymer [14]; and (2) upper T_g, representing the glass to rubber transition of nematically ordered molecules [14]. Previous research by Freeman's group [13,14] demonstrated that low temperature annealing at 140 °C for 1 h resulted in the formation of nematic structure but no crystals. Thus, in HIQ-40 annealing at low T_a results in 'nematically ordered material' [14], with true three-dimensional crystals forming later (longer annealing times) or at higher T_a.

Fig. 11 is a diagram that is our suggestion for depicting the dependence of structure of HIQ-40 on annealing temperature. At low T_a, the sample is being annealed from a state of low molecular mobility. First, the temperature increases above T_g (about 120 °C) to T_a, and widely scattered nematic domains form from isotropic liquid, as shown in Fig. 11(a). At $T_a = T_c$, the most mobile of these domains can become crystallized (Fig. 11(b)). Upon cooling HIQ-40 to room temperature, this sample will contain crystals (that show a Bragg long period), locally ordered nematic domains that could not crystallize at T_a, and isotropic domains that could not become nematic at T_a.

Upon reheating a sample previously treated at low T_a, once the temperature increases above T_a, more crystals can form during the scan, but eventually all the crystals will melt (Fig. 11(c)). This releases constraints on the disordered regions, allowing further transformations to occur. Above the melting point of the crystals, the first observed liquid crystal phase transition, at T_{lc1}, results from the crystal melt transforming to locally ordered nematic (Fig. 11(d)). A second liquid crystalline transition occurs at T_{lc2} when the less mobile portions of the sample (those unable to form crystals or nematic regions at low temperature) transform to nematic order (Fig. 11(e)). In both (d) and (e), the birefringence will be increased by the additional liquid crystalline order. The size scale of the ordered domains is such that we see their signature in the SAXS regime at low

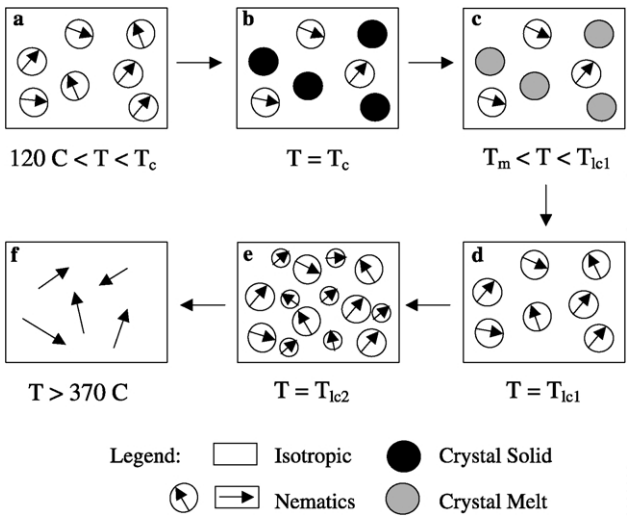

Fig. 11. Model for structure formation in HIQ-40. The arrows between frames indicate increasing temperature. (a) Above the glass transition, scattered nematic regions form. (b) Crystallization occurs in the most mobile nematic regions at T_c. (c) Crystals melt at T_m. (d) Melt becomes nematically ordered at T_{lc1}. (e) Nematic domains form at T_{lc2}. (f) More uniform nematic forms.

s-vector. Finally, at high temperatures the domains with differing local nematic order become a more uniform nematic. Any domains that remain now are of a size scale that could not be seen in SAXS. The much higher temperature nematic-to-isotropic transition was not observed in the present study.

The crystallization and melting temperatures depend strongly upon T_a and range widely over the temperatures studied (e.g. T_m ranges from 257 to 338 °C, as shown in Table 1). We conclude from our thermal analysis that the crystalline phase may reorganize during heating leading to increase in the melting temperature. The liquid crystalline transitions, however, are restricted to more narrow temperature intervals: both T_{lc1} and T_{lc2} occur over relatively narrow temperature ranges of about 20 degrees. The sharpness of the liquid crystalline transitions, in comparison to the crystalline ones, suggests that the liquid crystal phase formation in HIQ-40 is driven principally by thermodynamics, and not by kinetics.

The sample treated at 290 °C is different, since this high T_a is actually located within the melting endotherm range. Long annealing in the melt state creates highly birefringent ordered liquid crystal structures but no crystals. Crystals form immediately during cooling to room temperature, but are widely scattered and exhibit no Bragg period. Upon reheating, above 290 °C the crystals are now already melted, and locally ordered nematic domains form and show a very strong SAXS scattering peak without much change in birefringence. Disappearance of the domain structure at about 350 °C occurs with transformation of the remaining isotropic material into ordered nematic (Fig. 11(e)–(f)). With the elimination of domains, the nematic fills the whole sample, and the SAXS peak disappears while the overall birefringence increases sharply.

4. Conclusions

Cold-crystallization of HIQ-40 thermoplastic co-polyester films has been shown to have large impact on its structure. When initially isotropic films are cold crystallized at temperatures T_a, from 130 to 290 °C, the glass transition shifts towards lower temperatures as T_a increases. This is evidence that the crystals introduced at higher T_a are produced from a more mobile state, and therefore do not constrain the amorphous phase as much as when the crystals are formed at lower T_a.

For crystallization temperatures below 290 °C, HIQ-40 exhibits a clear Bragg long period that shifts to larger spacing (i.e. occurs at lower *s*-vector) as temperature increases during heating. The overall SAXS intensity generally increases during heating and reaches a maximum just at the temperature marking the boundary between the crystal melting transitions and the crystal to nematic transition (lower temperature dashed line in Figs. 2(b), 9 and 10). The formation of locally ordered nematic phase causes: (a) decrease in SAXS intensity, signaling a reduction in the electron density contrast between scattering phases, and, (2) increase in transmitted light intensity, due to formation of entities of higher birefringence. Above the crystal to nematic transition (upper temperature dashed line in Figs. 2(b), 9 and 10) SAXS invariant and transmitted light intensity increase in all samples treated below 290 °C.

The sample treated at 290 °C must be described separately, since its behavior by all experimental methods was different from that of samples treated at lower temperatures. Annealing at 290 °C occurs within the melting endotherm of the previous crystal population (formed in the non-pretreated 'parent' material during heating to T_a.). The crystals in this sample form primarily during cooling, and do not form during the isothermal period at T_a. The crystals seen in the WAXS scans melt at low temperature, below 290 °C, verifying that their crystallization occurred on cooling. Furthermore, these crystals exhibit no strong Bragg scattering in SAXS, so they are either not organized into periodic stacks or the stack period is too large to be observed with our equipment. As temperature increases above the lower temperature dashed line (see Figs. 2(b), 9 and 10) the principal endothermic event is seen, resulting from the transition to the nematic phase. This transition is accompanied by a strong increase in SAXS intensity, suggesting the formation of two-phase structure. Thus, thermal annealing within the original crystal's melting endotherm is likely to pre-condition the melt to form nematic domains when the temperature is increased above T_a.

Acknowledgements

This research was supported by the National Aeronautics and Space Administration Grant NAG-8-1480.

References

[1] Donald A, Windle A. Liquid crystalline polymers. Cambridge, GB: Cambridge University Press; 1995.
[2] Blundell D. Polymer 1982;23:359–64.
[3] Erdemir AB, Johnson DJ, Tomka JG. Polymer 1986;27:441–7.
[4] Butzbach G, Wendorff J, Zimmermann H. Polymer 1986;27:1337–44.
[5] Erdemir AB, Johnson DJ, Karacan I, Tomka JG. Polymer 1988;29:597–604.
[6] Lemmon T, Hanna S, Windle A. Polym Commun 1989;30:2–4.
[7] Hoff M, Keller A, Odell JA, Percec V. Polymer 1993;34:1800–5.
[8] Dainelli D, Chapoy L. Macromolecules 1993;26:385–90.
[9] Makhija S, Jaffe MJ. Appl Polym Sci 1994;53:609–20.
[10] Cao J, Erdemir AB, Karacan I, Tomka JG. Polymer 1995;36(24):4695–701.
[11] Menczel J, Jaffe M, Saw C. J Therm Anal 1996;46:733–52.
[12] Park J, Paul D, Haider I, Jaffe M. J Polym Sci: Part B Polym Phys 1996;34:1741–5.
[13] McDowell C, Freeman B, McNeely G, Haider M, Hill A. J Polym Sci: Part B Polym Phys 1998;36(16):2981–3000.

[14] Cantrell G, McDowell C, Freeman B, Noel C. J Polym Sci: Part B Polym Phys 1999;37:505–22.
[15] Collins T, Davies G, Ward I. Polym Adv Technol 2001;12:544.
[16] Jaffe M. Polym Prepr 1999;40(1):574.
[17] Xu H, Ince BS, Cebe P. J Polym Sci: Part B Polym Phys 2003;41(23): 3026–36.
[18] Huo PP, Cebe P. Macromolecules 1992;25:902–9.
[19] Ivanov DA, Legras R, Jonas AM. Macromolecules 1999;32:1582–92.
[20] Fougnies C, Damman P, Dosiere M, Koch MHJ. Macromolecules 1997;30:1392–9.
[21] Balta-Calleja FJ, Vonk CG. X-ray scattering of synthetic polymers. New York, NY: Elsevier Science Publisher; 1989. p. 241–94.
[22] Cebe P. Introduction to scattering from polymers. In: Cebe P, Hsiao B, Lohse D, editors. Scattering from polymers: characterization by X-rays, neutrons and light. Washington, DC: American Chemical Society; 2000. p. 2–22.
[23] MATLAB™ The Mathworks, Natick, MA; 2000.
[24] Strobl G, Schneider M. J Polym Sci: Polym Phys Ed 1980;18: 1343–59.
[25] Georgiev G, Berns D, Cebe P. Proceedings of the national aeronautic and space administration, microgravity materials conference. Huntsville: Alabama; 2000. p. 35–6.
[26] Cebe P, Dai P, Georgiev G, Feinberg B, Gilfoy N, Capel M. Polym Prepr 2002;43(1):242.
[27] Oldenbourg R, Mei G. J Microsc 1995;180(2):140–7.
[28] Friedman L. Private communication; 1997.
[29] Georgiev G, Cebe P, Capel M. J Mater Sci 2001;36(6):1349–61.
[30] Huo PP, Cebe P. Colloid Polym Sci 1992;270(9):840–52.
[31] Huo PP, Cebe P. J Polym Sci: Part B Polym Phys 1992;30:239–50.
[32] DeGennes PD, Proust J. Physics of liquid crystals. Oxford: Oxford University Press; 1995.
[33] Dai P, Cebe P, Capel M. J Polym Sci: Part B Polym Phys 2002;40: 1644–60.
[34] Jonas A, Russel T, Yoon D. Colloid Polym Sci 1994;272:1344–51.